

Supplemental Materials: Topological phase transformations and intrinsic size effects in ferroelectric nanoparticles

John Mangeri,^{*,†} Yomery Espinal,[‡] Andrea M. Jokisaari,[¶] S. Pamir Alpay,^{‡,†}
Serge Nakhmanson,^{‡,†} and Olle G. Heinonen^{*,§,¶}

[†]*Department of Physics, University of Connecticut, Storrs, Connecticut 06269, USA*

[‡]*Department of Materials Science & Engineering and Institute of Material Science, University of Connecticut, Storrs, Connecticut 06269, USA*

[¶]*Center for Hierarchical Material Design, Northwestern-Argonne Institute of Science and Engineering, Northwestern University, Evanston, Illinois 60208, USA*

[§]*Material Science Division, Argonne National Laboratory, Lemont, Illinois 60439, USA*

E-mail: john.mangeri@uconn.edu; heinonen@anl.gov

Methods

Below we summarize the thermodynamic approach for simulating the coupled polar-elastic behavior of the ferroelectric inclusion embedded in the linear dielectric-elastic medium. Computational domain of the problem is split into two volumes – a sphere volume Ω_{FE} of the inclusion at the center of a cube volume Ω_{M} representing the surrounding matrix. The outer bounding surfaces of the Ω_{M} volume are denoted $\partial\Omega_{\text{M}}$, while the surface of the inclusion volume Ω_{FE} is denoted $\partial\Omega_{\text{FE}}$. We assume a coherent interface between the inclusion and outside medium.

The finite element model variants are meshed with tetrahedrons with CUBIT.¹ The unstructured

mesh size for the ferroelectric subdomain is chosen such that there are approximately 2 – 5 elements across the domain wall length scale. Outside of the sphere, no such constraint is held, and the mesh is allowed to coarsen as the radial distance is traversed to the boundary to improve computational efficiency. The ratio of the coarse boundary mesh size to sphere mesh size is kept relatively fixed throughout these calculations.

System energies

In a ferroelectric (FE) material, in some volume Ω_{FE} , spontaneous polarization arises at temperatures below the Curie temperature, T_C .^{2,3} By expanding the free energy density in the order parameters, one can show that the total free energy of a system, \mathcal{F} can be written as

$$\mathcal{F} = \int_{\Omega_{\text{FE}}} f d^3\mathbf{r} = \int_{\Omega_{\text{FE}}} [f_{\text{elastic}} + f_{\text{bulk}} + f_{\text{wall}} + f_{\text{elec}} + f_{\text{coupled}}] d^3\mathbf{r} \quad (1)$$

with

$$f_{\text{elastic}} \equiv \frac{1}{2} C_{ijkl} \varepsilon_{ij} \varepsilon_{kl}, \quad (2)$$

$$f_{\text{bulk}} \equiv \alpha_{ij} P_i P_j + \beta_{ijk} P_i P_j P_k + \gamma_{ijkl} P_i P_j P_k P_l + \omega_{ijklm} P_i P_j P_k P_l P_m + \delta_{ijklmn} P_i P_j P_k P_l P_m P_n, \quad (3)$$

$$f_{\text{wall}} \equiv G_{ijkl} \frac{\partial P_i}{\partial x_j} \frac{\partial P_k}{\partial x_l}, \quad (4)$$

$$f_{\text{elec}} \equiv -P_k \frac{\partial \Phi}{\partial x_k}, \quad (5)$$

and

$$f_{\text{coupled}} \equiv \frac{1}{2} q_{ijkl} \varepsilon_{ij} P_k P_l. \quad (6)$$

Here, $\mathbf{P}(\mathbf{r})$ is the polar field arising from ionic distortions on the lattice, $\varepsilon_{ij} = \frac{1}{2} (\partial u_i / \partial x_j + \partial u_j / \partial x_i)$ is the elastic strain tensor, $\mathbf{u}(\mathbf{r})$ is the displacement field and $\Phi(\mathbf{r})$ is the electrostatic potential. Einstein summation convention is assumed throughout this document for the Cartesian indices. Linear elastic energy density f_{elastic} accounts for linear elastic strain contributions to the total energy, with C_{ijkl} being the elastic stiffness tensor. f_{bulk} is bulk free energy, with expansion coefficients α_{ij} , β_{ijk} , γ_{ijkl} and so on determining the preferred magnitude and direction of the FE distortion in the unit cell below T_C . In addition, G_{ijkl} are gradient energy coefficients, and f_{wall} term expresses the energy contributions arising from local gradients in the polarization density. Electrostatic energy density f_{elec} represents the interaction of the FE polarization with internal and external electric fields. f_{coupled} governs the strength of the coupling between elastic strains and ionic distortions, represented by the electrostrictive tensor q_{ijkl} . Note that some works in the literature^{4,5} combine f_{elastic} and f_{coupled} into one term. Here, we have chosen to separate them out due to the fact that the result of the variational differentiation (with respect to \mathbf{P}) will only give nonzero results for terms that explicitly contain \mathbf{P} .

Materials parameters

Parameters α_{ij} , β_{ijk} , γ_{ijkl} , ω_{ijklm} , δ_{ijklmn} , G_{ijkl} , C_{ijkl} and $q_{ijkl} \equiv 2 C_{ijmn} Q_{mnkl}$, are material dependent, obey symmetries of the lattice, and in general can be dependent on temperature T . Group-theoretical methods^{6,7} can be used to reduce the number of these parameters to a minimum

by exploiting materials symmetries. In this work, we focus on canonical ferroelectrics PbTiO_3 (PT) and BaTiO_3 (BT), whose bulk and domain wall energy density expressions have the following forms:

$$\begin{aligned}
f_{\text{bulk}} = & \alpha_{11} (P_1^2 + P_2^2 + P_3^2) + \alpha_{11} (P_1^4 + P_2^4 + P_3^4) \\
& + \alpha_{12} (P_1^2 P_2^2 + P_2^2 P_3^2 + P_1^2 P_3^2) + \alpha_{111} (P_1^6 + P_2^6 + P_3^6) \\
& + \alpha_{112} [P_1^4 (P_2^2 + P_3^2) + P_2^4 (P_1^2 + P_3^2) + P_3^4 (P_1^2 + P_2^2)] \\
& + \alpha_{123} (P_1^2 P_2^2 P_3^2),
\end{aligned} \tag{7}$$

and

$$\begin{aligned}
f_{\text{wall}} = & \frac{1}{2} G_{11} \left[\left(\frac{\partial P_x}{\partial x} \right)^2 + \left(\frac{\partial P_y}{\partial y} \right)^2 + \left(\frac{\partial P_z}{\partial z} \right)^2 \right] \\
& + G_{12} \left[\frac{\partial P_x}{\partial x} \frac{\partial P_y}{\partial y} + \frac{\partial P_y}{\partial y} \frac{\partial P_z}{\partial z} + \frac{\partial P_x}{\partial x} \frac{\partial P_z}{\partial z} \right] \\
& + \frac{1}{2} G_{44} \left[\left(\frac{\partial P_x}{\partial y} + \frac{\partial P_y}{\partial x} \right)^2 + \left(\frac{\partial P_y}{\partial z} + \frac{\partial P_z}{\partial y} \right)^2 + \left(\frac{\partial P_x}{\partial z} + \frac{\partial P_z}{\partial x} \right)^2 \right] \\
& + \frac{1}{2} G'_{44} \left[\left(\frac{\partial P_x}{\partial y} - \frac{\partial P_y}{\partial x} \right)^2 + \left(\frac{\partial P_y}{\partial z} - \frac{\partial P_z}{\partial y} \right)^2 + \left(\frac{\partial P_x}{\partial z} - \frac{\partial P_z}{\partial x} \right)^2 \right].
\end{aligned} \tag{8}$$

For the bulk free energy that describes the energetics of the phase transition, only sixth order expansions are used, as such expansions are sufficient to reproduce the behavior of both PT and BT within the temperature range considered here.⁸ The bulk free energy coefficients for the two materials are listed in Table 1. The gradient (exchange coupling) free energy coefficients are presented in Table 2. For PT, the results in the main paper are obtained using PT set I, unless otherwise noted.

The choice of both PT and BT as FE materials of interest is partly motivated by their distinct

response to mechanical strains. In this problem, mechanical response arises due to strain transfer from the outside elastic matrix and self-strain within the inclusion (both of these play an important role in stabilizing the observed polarization textures). PT displays lower electrostriction but higher spontaneous polarization at room temperature $P_s^{\text{PT}} \simeq 0.75 \text{ C/m}^2$ than BT ($P_s^{\text{BT}} \simeq 0.26 \text{ C/m}^2$). The choice of matrix materials enveloping the inclusion, SrTiO₃ (ST), amorphous silica (*a*-SiO₂), and vacuum is primarily motivated by their dielectric strength ($\epsilon_m = 300, 2.6, \text{ and } 1$ respectively). We assume an isotropic (and linear) dielectric medium. The medium is also treated as elastic, with the exception of the vacuum case. The elastic stiffness tensor parameters listed in Table 3 primarily come from Refs. 9–11 and are presented in Voight notation.¹² For calculations of inclusions embedded in the ST matrix, elastic constants were averaged as $C_{11}, = C_{33} = 2\mu + \lambda$, $C_{12} = C_{13} = \lambda = 99.7 \text{ GPa}$, and $C_{44} = C_{66} = \mu = 109.6 \text{ GPa}$,^{9,11} which is a reasonable experimentally relevant assumption, since Ω_M is a much larger volume than the spherical inclusion and likely not to be single crystal.

Table 1: Ferroelectric material parameters used in this work for PbTiO₃ and BaTiO₃ at room temperature, $T = 293 \text{ K}$. Elastic stiffness and electrostrictive tensor coefficients are given in Voight notation.¹² Sixth order expansions of the bulk free energy are used for both materials. All coefficients are given in SI units.

	PbTiO ₃	BaTiO ₃	Ref.
α_1	-7.1×10^7	-2.94×10^7	3
α_{11}	-7.3×10^7	-6.71×10^8	-
α_{12}	7.5×10^8	3.23×10^8	-
α_{111}	2.6×10^8	8.28×10^9	-
α_{112}	6.1×10^8	4.47×10^9	-
α_{123}	-3.7×10^9	4.91×10^9	-
ϵ_b	10	7.35	13,14
Q_{11}	0.089	0.11	4,15
Q_{12}	-0.026	-0.045	-
Q_{33}	0.034	0.059	-
C_{11}	281	116	9,11
C_{12}	116	104	-
C_{33}	97	120	-

Table 2: Different sets of gradient energy parameters, G_{ijkl} , presented in Voigt notation¹² for G_{ij} and G_{110} in units of $10^{-10}\text{C}^{-2}\text{m}^4\text{N}$. We utilize three different sets of parameters from the literature to evaluate how polar properties of PT inclusions are affected by their choice. For BT, only one set of gradient terms due to Hlinka and collaborators is used.

G_{ijkl}	PT set I ^{4,5}	PT set II ¹⁶	PT set III ¹⁷	BT ¹⁴
G_{110}	1.73	1.73	1.73	1.0
G_{11}/G_{110}	0.6	1.6	2.0	5.1
G_{12}/G_{110}	0.0	0.0	0.0	0.0
G_{44}/G_{110}	0.3	0.8	1.0	0.2
G'_{44}/G_{110}	0.3	0.8	1.0	0.2

Table 3: Linear dielectric material parameters used in this work for SrTiO_3 and $\alpha\text{-SiO}_2$ at room temperature, $T = 293$ K. Medium dielectric constants are assumed to be isotropic and are given in units of the relative permittivity. Elastic stiffness tensor coefficients are given in Voigt notation¹² in units of GPa. Elastic stiffness tensors of the amorphous silica are obtained from averaging data presented in Ref.¹⁰

	SrTiO_3	$\alpha\text{-SiO}_2$	vacuum	Ref
C_{11}	319	63	-	10, 9, 11
C_{12}	100	6	-	-
C_{44}	110	28	-	-
ϵ_m/ϵ_0	300	2.6	1	18, 10

Gradient-flow approach

FERRET¹⁹ is an open-source code-package for simulating ferroelectric nano structures based on the multi-physics finite element framework MOOSE.²⁰ In contrast to spectral methods^{4,5,15,17} that rely on regular parallelepiped meshes, the method utilized here implements a real-space approach based on irregular unstructured meshes, which allows it to process irregular geometries (using the LIBMESH²¹ library).

Evolution of the polarization field, \mathbf{P} , in the inclusion in a linear dielectric is described by the time-dependent Landau-Ginzburg-Devonshire (TDLGD) equation,

$$-\gamma \frac{\partial \mathbf{P}}{\partial t} = \frac{\delta}{\delta \mathbf{P}} \int_{\Omega_{\text{FE}}} d^3\mathbf{r} f(\mathbf{P}), \quad (9)$$

where γ is a time-scaling parameter related to domain-wall mobility.²²

The variable γ is set to unity in this investigation and, therefore, the TDLGD equation is solved in an arbitrary scaled time. This is because in real materials, elastic strain usually relaxes much faster than the polarization,²³ we assume that the local displacement field $\mathbf{u}(\mathbf{r})$ instantaneously adjusts to the current state of the polarization field \mathbf{P} . This results in the following mechanical equilibrium condition for the system that must be satisfied at every time step of the evolution of \mathbf{P} :

$$\frac{\partial}{\partial x_j} [C_{ijkl} (\varepsilon_{kl} - Q_{ijmn} P_m P_n)] = 0 \quad (10)$$

Furthermore, the evolution of \mathbf{P} is also coupled with that of the local (internal) electrostatic potential Φ by the Poisson equation:

$$\nabla \cdot (\epsilon_b \nabla \Phi) = \rho_b. \quad (11)$$

Here, ρ_b is bound volume charge that is equal to $-\nabla \cdot \mathbf{P}$. Solving Eq. 11 accounts for the long-range Coulombic interactions within the system, including the potential emergence of the so-called depolarization field that originates from the presence of unscreened charges on the inclusion surface

$\partial\Omega_{\text{FE}}$. Parameter ϵ_b , sometimes called the background dielectric constant, represents contributions from core electrons to the dielectric response of the ferroelectric^{13,14,24} that can moderately screen the polarization field. In previous investigations, this parameter has been varied widely for both PT and BT: $\epsilon_b/\epsilon_0 = 4$ to 70.^{15,17,25} We choose $\epsilon_b/\epsilon_0 = 10$ ¹³ and 7.35¹⁴ for PT and BT, respectively, i.e., we use values that are close to those of the electronic contribution ϵ^∞ to the total dielectric permittivity²⁴ for these materials. It should also be noted that varying this parameter does not seem to affect the results presented in this work.

The state of the dielectric matrix surrounding the FE inclusion is governed by a different set of equations. ST and *a*-Si are assumed to be linear dielectrics, with an isotropic dielectric permittivity ϵ_m . The following equation must be satisfied for the electrostatic potential within the matrix:

$$\nabla (\epsilon_m \cdot \nabla \Phi) = 0, \quad (12)$$

complemented by the stress divergence equation:

$$\frac{\partial \sigma_{ij}}{\partial x_j} = 0. \quad (13)$$

The system boundary conditions include vanishing elastic distortions far away from the inclusion, i.e., ($\mathbf{u} \rightarrow 0$) at $\partial\Omega_M$. The same governing equations exist in the vacuum region, except \mathbf{u} is nonexistent. Also, a short-circuited⁵ boundary condition on Φ is chosen for the pair of opposite sides of the cube Ω_M with plane normals oriented along $[00 \pm 1]$. By adjusting the values of Φ on these two sides, an external field can be applied. In the absence of the applied field, $\Phi \rightarrow 0$ is enforced on the boundary planes of Ω_M (which are assumed to be far away from the inclusion). Consistency checks were done to make sure that, as a function of the size of the inclusion sphere, the internal (fringing) electrostatic potential and the strain fields originating from elastic distortions did in fact vanish at the boundaries of the computational domain. Larger matrix domains were needed to ensure fringing fields from larger spheres vanished.

Our approach implemented in FERRET¹⁹ allows for solving coupled Eqs. 9 through 10 self-

consistently for the displacement vector field $\mathbf{u}(\mathbf{r})$, polarization vector field $\mathbf{P}(\mathbf{r}, t)$, and electrostatic potential scalar field $\Phi(\mathbf{r})$. These equations are first separated into their respective subdomains, and then cast into the weak-form suitable for Galerkin’s finite element method. A fully implicit time integration is implemented in a Newton-Raphson scheme. The iterative Generalized Minimal Residual²⁶ algorithm is used to solve the block diagonal preconditioned linear system. The full solve utilizes convergence to within 1×10^{-6} relative nonlinear residual tolerance.

Since Eq. 9 is a partial differential equation that depends on time, an initial condition for evolving the \mathbf{P} field must be chosen. For this particular problem, we adopt an initial condition that resembles a paraelectric state of the material at some $T > T_C$, which forces \mathbf{P} to be randomly distributed near zero. The rationale for choosing such random paraelectric initial condition (RPEIC) is to ensure that there is no “memory” bias in the domain structure that forms as the energy is dissipated out of the system by the gradient descent algorithm. Such condition is widely used in phase field modeling of FE materials.^{4,5,15} The temperature is then immediately set below T_C and the TDLGD Eq. 9 is evolved (by solving 11 and 10 at each time step) until a (local) energy minimum has been found. The simulation exit criterion is achieved when the difference in the magnitude of the total energy is below 0.1% during the two consecutive time steps.

Quasi-static poling

In order to apply an electric field to the particle and calculate its field-dependent polarization response, we use a quasi-static poling procedure. This procedure involves an application of the electric field \mathbf{E} along the $[00\pm 1]$ crystallographic direction. The TDLGD equations are then evolved, as discussed above, so that an appropriate energy minimum is found in the presence of the applied field. In order to improve the computational efficiency of these polarization curve calculations, the converged solution at the previous value of the field is used as an initial solution at the current

value of the field in the following equation,

$$-\gamma \frac{\partial \mathbf{P}}{\partial t} = \frac{\delta}{\delta \mathbf{P}} \int_{\Omega} d^3 \mathbf{r} f(\mathbf{P}) + \xi \cdot \hat{\mathbf{P}}, \quad (14)$$

where ξ is a random noise term with gaussian distribution which can effectively be related to thermal fluctuations in a real experiment. The introduction of the noise term is helpful in ejecting the initial solution out of its original energy well.

Supplementary results

Core topologies

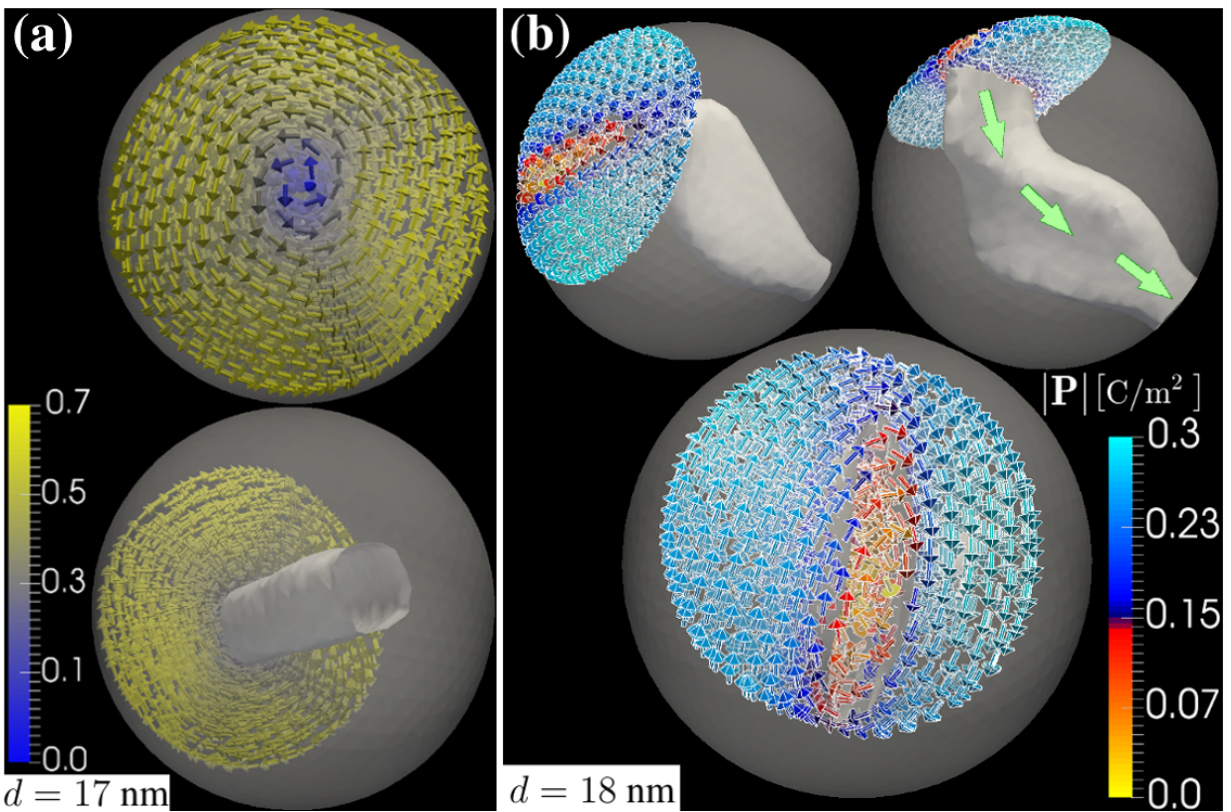


Figure 1: Panel (a) depicts cuts through the polarization texture at $|\mathbf{P}| = 0.35 \text{ C/m}^2$ for the PT/ST inclusion with $d = 17 \text{ nm}$ at zero applied field. The contour of the vortex core is also shown. In panel (b), the same information is presented for the 18 nm BT/ST inclusion at $|\mathbf{P}| = 0.17 \text{ C/m}^2$.

Electrostrictive influence on polarization texture

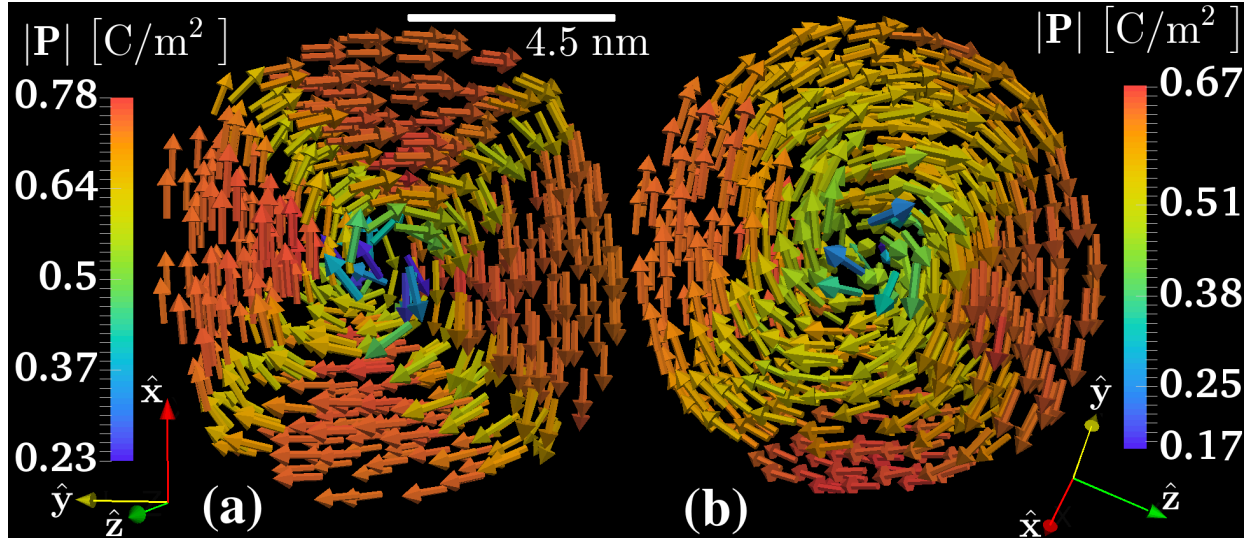


Figure 2: Image slices perpendicular to the vortex core, showing polarization texture differences between the states with (a) no electrostrictive coupling and (b) active electrostrictive coupling in a $d = 9$ nm PT particle embedded in the ST matrix.

To examine the effects of the electrostrictive coupling on the equilibrium ferroelectric polarization, we perform two calculations, one with the electrostrictive tensor components set to zero, and the other with the “active” electrostrictive tensor, using identical RPEIC for both calculations. The vortex-like structure that forms in the absence of electrostrictive coupling resembles a Landau flux-closure domain^{27,28} mapped onto spherical geometry, as shown in the Supplementary Fig. 2(a) for the PT/ST system with $d = 9$ nm. On the other hand, the presence of the electrostrictive coupling softens the sharp 90° domain walls, producing a more rounded vortex-like state, as observed in Ref. 29–33, while slightly depressing the value of $|\mathbf{P}|$ at the surface (by about 13%) — as can be seen by the comparison of panels (a) and (b) of the Supplementary Fig. 2. The vortex core textures also differ, with the polar directors pointing out-of-plane in the panel (a), while being strictly in-plane in the panel (b).

Evaluating vorticity of polarization textures

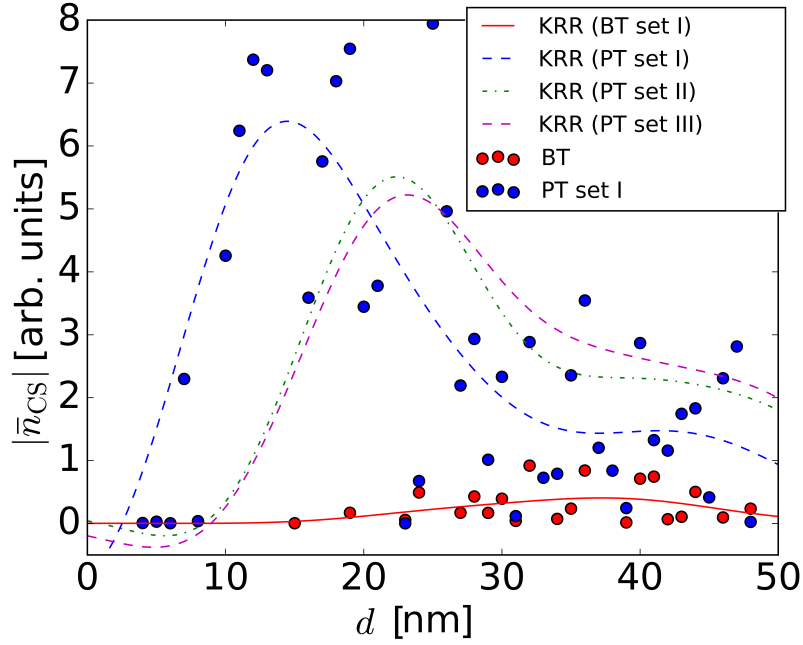


Figure 3: Kernel ridge regression (KRR) fits for the magnitude of the average Chern number density $|\bar{n}_{CS}|$ as a function of the particle size. Flattened out curve regions at large d indicate the presence of multidomains in the polarization texture. Note that such flattening occurs at different particle sizes, compared to the F_{wall} dependence presented in Fig. 2 in the main text, indicating that these two measures of system vorticity are not completely equivalent.

Easy and hard axis poling in the monodomain system

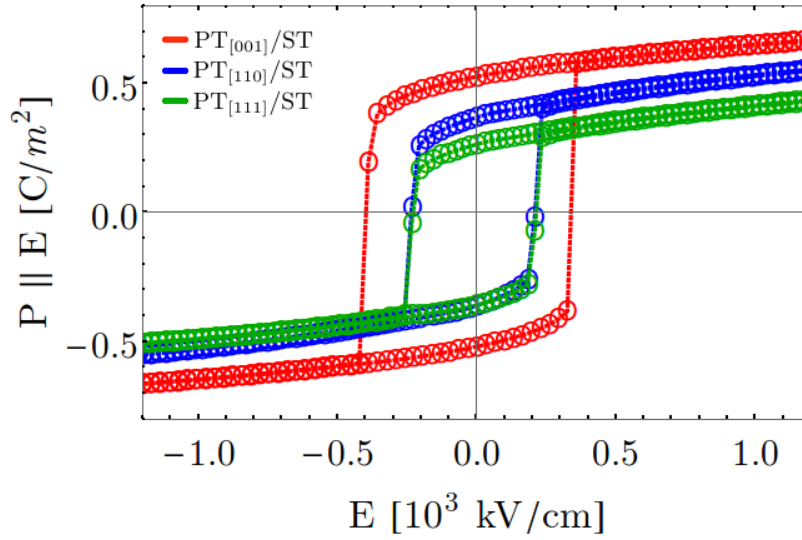


Figure 4: Applied field-dependent polarization curves for a PT particle with $d < d_v$ embedded in the ST dielectric medium. Electric field is applied along the \hat{z} direction, while different crystallographic orientations of the PT unit cell are aligned with the field by rotating the particle: *Red curve*: [001], or easy polar axis, corresponding to the preferred orientation of \mathbf{P} in bulk PT (space group $P4mm$); *Blue curve*: [110] orientation; *Green curve*: [111] orientation. The latter two orientations can be considered as hard polar axes in bulk PT, with corresponding average polarizations depressed, compared to the easy-axis case.

References

- (1) CUBIT meshing software is developed by Sandia National Laboratories and is available at <https://cubit.sandia.gov/>.
- (2) Lines, M. E.; Glass, A. M. *Principles and Applications of Ferroelectrics and Related Materials*; Clarendon, Oxford, 1977.
- (3) Rabe, K. M.; Ahn, C. H.; Triscone, J.-M. *Physics of Ferroelectrics: A Modern Perspective*; Springer-Verlag, Berlin, 2007.
- (4) Li, Y. L.; Hu, S. Y.; Liu, Z. K.; Chen, L.-Q. *Appl. Phys. Lett.* **2001**, 78, 24.
- (5) Li, Y. L.; Hu, S. Y.; Liu, Z. K.; Chen, L.-Q. *Appl. Phys. Lett.* **2002**, 81, 3.
- (6) El-Batanouny, M.; Wooten, F. *Symmetry in Condensed Matter Physics: A Computational Approach*; Cambridge, 2008.
- (7) Cao, W. *Ferroelectrics* **2008**, 375, 28–39.
- (8) Lu, H., X. Li; Cao, W. *J. Appl. Phys.* **2013**, 114, 224106.
- (9) Jain, A.; Ong, S. P.; Hautier, G.; Chen, W.; Richards, W. D.; Dacek, S.; Cholia, S.; Gunter, D.; Skinner, D.; Ceder, G.; Persson, K. A. *APL Materials* **2013**, 1(1).
- (10) Pabst, W.; Gregorova, E. *Ceramics* **2013**, 57, (3) 167–184.
- (11) de Jong, M.; Chen, W.; Angsten, T.; Jain, A.; Notestine, R.; Gamst, A.; Sluiter, M.; Ande, C. K.; van der Zwaag, S.; Plata, J. J.; Toher, C.; Curtarolo, S.; Ceder, G.; Persson, K. A.; Asta, M. *Scientific Data* **2015**, 2:, 150009.
- (12) Nye, J. F. *Physical Properties of Crystals*; Oxford University Press Inc., 1985.
- (13) Mokřý, P.; Sluka, T. *Phys. Rev. B.* **2016**, 93.
- (14) Hlinka, J.; Marton, P. *Phys. Rev. B.* **2006**, 74, 104104.

- (15) Gu, Y.; Li, M.; Morozovska, A. N.; Wang, Y.; Eliseev, E. A.; Gopalan, V.; Chen, L.-Q. *Phys. Rev. B* **2014**, *89*, 174111.
- (16) Wang, J.; Shi, S.-Q.; Chen, L.-Q.; Li, Y.; Zhang, T.-Y. *Acta Mater.* **2004**, 749–764.
- (17) Hong, L.; Soh, A. K. *Appl. Phys. Lett.* **2011**, *81*, 342–347.
- (18) Müller, K. A.; Burkard, H. *Phys. Rev. B* **1979**, *19*, 7.
- (19) The FERRET code-repository is developed within the open-source MOOSE environment²⁰ and is available at <https://bitbucket.org/mesosience/ferret>.
- (20) Gaston, D.; Newman, C.; Hansen, G.; Lebrun-Grandié, D. *Nucl. Eng. Design* **2009**, *239*, 1768.
- (21) Kirk, B. S.; Peterson, J. W.; Stogner, R. H.; Carey, G. F. *Eng. with Comp.* **2006**, *22*(3-4), 237–254.
- (22) Meng, Q.; Han, M.-G.; Tao, J.; Xu, G.; Welch, D. O.; Zhu, Y. *Phys. Rev. B* **2015**, *91*, 054104.
- (23) Li, Y.; Hu, S.; Liu, Z.; Chen, L. *Acta Mater.* **2002**, *50*, 395 – 411.
- (24) Baroni, S.; Gironcoli, S.; Corso, A. D. *Rev. Mod. Phys.* **2001**, *73*, 515.
- (25) Eliseev, E. A.; Kalinin, S. V.; Morozovska, A. N. *J. Appl. Phys.* **2015**, *117*, 034102.
- (26) Saad, Y.; Schultz, M. *J. Sci. Stat. Comp.* **1986**, *7*, 856–869.
- (27) Hubert, A.; Schäfer, R. *Magnetic Domains*; Springer-Verlag Berlin Heidelberg, 1998.
- (28) Raabe, J.; Quitmann, C.; Back, C. H.; Nolting, F.; Johnson, S.; Buehler, C. *Phys. Rev. Lett.* **2005**, *94*, 217204.
- (29) Naumov, I.; Bratkovsky, A. M. *Phys. Rev. Lett.* **2008**, *101*, 107601.
- (30) Gruverman, D., A. Wu; Fan, H.-J.; Vrejoiu, I.; Alexe, M.; Harrison, R. J.; Scott, J. F. *J. Phys.: Condens. Matter* **2008**, *20*, 342201.

(31) Levanyuk, A. P.; Blinc, R. *Phys. Rev. Lett.* **2013**, *11*, 097601.

(32) Martelli, P.-W.; Mefire, S.; Luk'Yanchuk, I. A. *Euro. Phys. Lett.* **2015**, *111*, 50001.

(33) Nahas, Y.; Prokhorenko, S.; Louis, L.; Gui, Z.; Kornev, I.; Bellaiche, L. *Nature Comm.* **2015**, *6*, 8542.